Open access • Journal Article • DOI:10.1007/BF02646145

role of crack tip shielding in the initiation and growth of long and small fatigue cracks in composite microstructures — Source link

Jian Ku Shang, J. L. Tzou, Robert O. Ritchie

Institutions: University of California, Berkeley

Published on: 01 Sep 1987 - Metallurgical and Materials Transactions A-physical Metallurgy and Materials Science (Springer-Verlag)

Topics: Crack closure, Crack growth resistance curve, Stress concentration and Fracture mechanics

Title

ROLE OF CRACK TIP SHIELDING IN THE INITIATION AND GROWTH OF LONG AND SMALL FATIGUE CRACKS IN COMPOSITE MICROSTRUCTURES

Authors

Shang, J.K.
Tzou, J.L.
Ritchie, R.O.

Publication Date

1986-09-01

LBL-21895
Preprint

Lawrence Berkeley Laboratory
UNIVERSITY OF CALIFORNIA

Materials & Chemical Sciences Division

Submitted to Metallurgical Transactions A

ROLE OF CRACK TIP SHIELDING IN THE INITIATION AND GROWTH OF LONG AND SMALL FATIGUE CRACKS IN COMPOSITE MICROSTRUCTURES

J.K. Shang, J.-L. Tzou, and R.O. Ritchie

September 1986

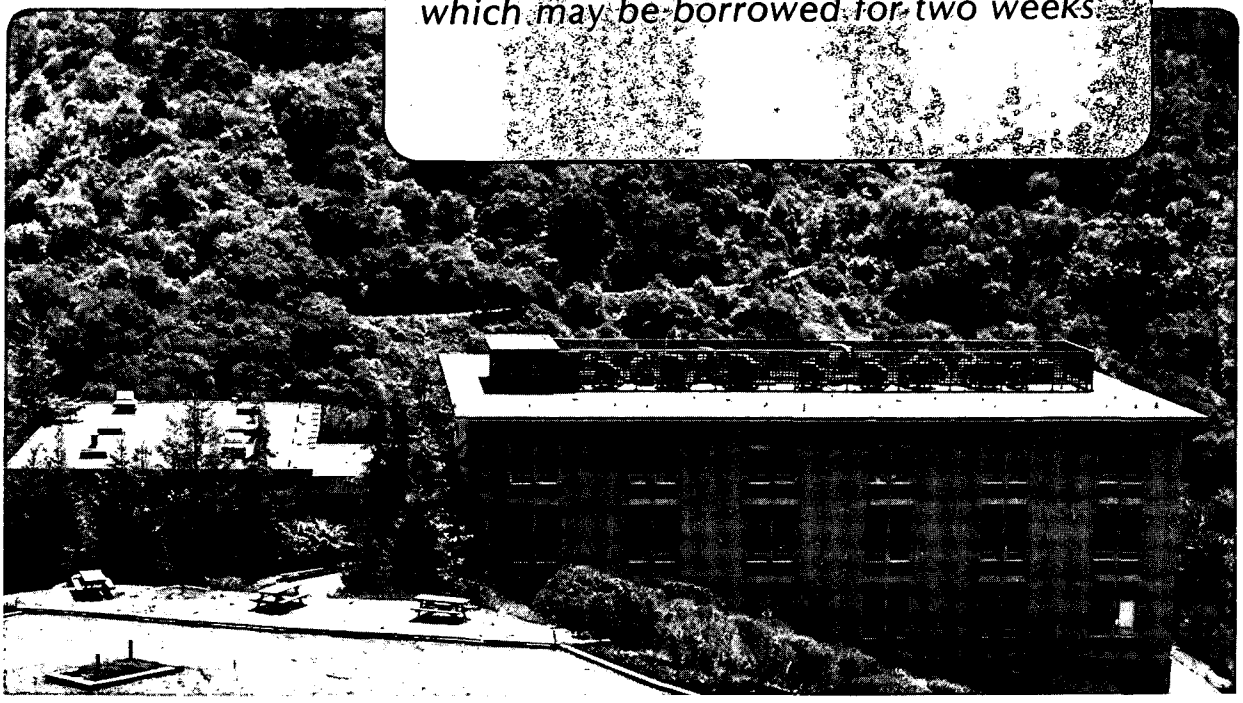

Prepared for the U.S. Department of Energy under Contract DE-AC03-76SF00098

DISCLAIMER

LBL-21895

ROLE OF CRACK TIP SHIELDING IN THE INITIATION AND GROWTH OF LONG AND SMALL FATIGUE CRACKS IN COMPOSITE MICROSTRUCTURES

by

Jian Ku Shang, J.-L. Tzou,* and R. O. Ritchie

Materials and Chemical Sciences Division,
Lawrence Berkeley Laboratory,
and
Department of Materials Science and Mineral Engineering,
University of California, Berkeley, CA 94720

*National Semiconductor Corporation, Santa Clara, CA 95051

September 1986

revised March 1987

submitted to Metallurgical Transactions A

This work was supported by the Director, Office of Energy Research, Office of Basic Energy Sciences, Materials Science Division of the U.S. Department of Energy under Contract No. DE-AC03-76SF00098.

ROLE OF CRACK TIP SHIELDING IN THE INITIATION AND GROWTH OF LONG AND SMALL FATIGUE CRACKS IN COMPOSITE MICROSTRUCTURES

Jian Ku Shang, J.-L. Tzou, and R. O. Ritchie

ABSTRACT

The role of crack tip shielding in retarding the initiation and growth of fatigue cracks has been examined in metallic composite microstructures (consisting of hard and soft phases), with the objective of achieving maximum resistance to fatigue. Specifically, duplex ferritic-martensitic structures have been developed in AISI 1008 and 1015 mild steels to promote shielding without loss in strength. The shielding is developed primarily from crack deflection and resultant crack closure, such that unusually high long crack propagation resistance is obtained. It is found that the fatigue threshold ΔK_{TH} in AISI 1008 can be increased by more than 100% to over 20 MPa$\sqrt{m}$, without sacrifice in strength, representing the highest ambient temperature threshold reported for a metallic alloy to date. Similar but smaller increases are found in AISI 1015. The effect of the dual-phase microstructures on crack initiation and

---

JIAN KU SHANG, J.-L. TZOU and R. O. RITCHIE are Graduate Student, former Graduate Student and Professor, respectively, with the Materials and Chemical Sciences Division, Lawrence Berkeley Laboratory, and the Department of Materials Science and Mineral Engineering, University of California, Berkeley, CA 94720. Mr. Tzou is now with National Semiconductor Corporation, Santa Clara, CA 95051.

small crack (10 to 1000 μm) growth, however, is markedly different, characteristic of behavior influenced by the mutual competition of intrinsic and extrinsic (shielding) "toughening" mechanisms. Accordingly, the composite microstructures which appear to show the highest resistance to the growth of long cracks, show the lowest resistance to crack initiation and small crack growth. In general, dual-phase steels are found to display remarkable fatigue properties, with fatigue limits as high as 58% of the tensile strengths and fatigue thresholds in the range of 13 to 20 MPa$\sqrt{m}$.

I. INTRODUCTION

Crack extension is generally considered to be driven by the presence of a **"crack driving force"** and opposed by the **resistance of the microstructure,** where the driving force is globally defined by a characterizing parameter, such as the stress intensity K_I, describing the dominant crack tip stress and deformation fields. It is thus the perception that toughening, or restriction of crack growth, is achieved by increasing the inherent microstructural resistance, e.g., by coarsening particle spacings, etc. (**intrinsic "toughening"***):

---

*"Toughening" is used here in a general sense to imply mechanisms which impede crack extension, and thus is applied to both sub-critical and critical behavior.

However, in many cases, the actual source of toughness arises from a process of **crack tip shielding,** where crack extension is impeded by mechanical, microstructural and environmental factors which locally reduce the crack driving force (**extrinsic "toughening"**) (1,2). Notable examples under monotonic loading are transformation toughening in ceramics (3,4) and ligament toughening in composites (5) (Fig. 1).

Crack tip shielding processes are also of importance under cyclic loading, but relate primarily to crack deflection (6) and crack closure from wedging, bridging and sliding phenomena between crack surfaces (7-15). Specific closure mechanisms can involve the wedging action of corrosion debris (8-10), fracture surface

asperities (11-13) and fluid pressure (14), and the presence of cyclic plasticity in the crack wake (15). With the exception of the latter, all are enhanced at low stress intensities due to smaller crack tip opening displacements (CTOD) and the greater tendency of cracks to follow a microstructurally-sensitive or crystallographic crack path.

For fatigue crack advance under small-scale yielding, the effect of shielding is locally to reduce the nominal range of stress intensity, ΔK, given by $K_{max} - K_{min}$, to some effective value, ΔK_{eff}, actually experienced at the tip, although computation of ΔK_{eff} depends critically on the dominant mechanism of shielding. For example, crack deflection produces a multiplicative reduction in Mode I stress intensities, i.e., ΔK is reduced by a decrease in K_{max} and a smaller decrease in K_{min}, which may be expected to have an equal effect throughout the range of growth rates (unless the crack path morphology changes). Bridging or sliding mechanisms, conversely, lower ΔK by a decrease in K_{max} and an **increase** in K_{min}. Most closure mechanisms, however, involve principally wedging, where ΔK is reduced by an effective increase in K_{min}. Here ΔK_{eff} is defined in terms of a stress intensity K_{cl} to cause first contact of the crack surfaces as $K_{max} - K_{cl}$ (1,7). These mechanisms predominate at lower growth rates where wedge sizes are comparable with CTODs.

Since shielding acts primarily on the wake of the crack, a direct implication is crack-size dependent behavior. This leads to resistance-curve fracture toughness behavior, where the driving force

to sustain cracking increases with an increase in crack length; anomalous **"small crack" behavior,** where at the same nominal driving force, small cracks propagate faster than long cracks, due to their higher local driving force from diminished shielding; and **a contrasting role of microstructural factors** in influencing crack initiation and small crack growth compared to long crack growth.

The objective of the present work is to show that by designing composite microstructures to promote crack tip shielding, exceptional fatigue crack growth properties can be achieved without compromise in strength or crack initiation resistance. This concept is demonstrated by utilizing duplex microstructures in common engineering mild steels to obtain fatigue thresholds higher than any known metallic material reported to date.

II. EXPERIMENTAL PROCEDURES

AISI-SAE 1008 and 1015 mild steels, of composition shown in Table I, were received as 22 mm thick hot rolled plate. Oversize specimen blanks were austenitized 1 h at 1100°C (to obtain a prior austenite grain size of $\sim$ 50 μm), air cooled to room temperature, and then intercritically annealed for 1 h before iced-brine quenching. The intercritical annealing temperatures were chosen between 760° and 850°C in order to vary both the volume fraction of martensite (between 25 and 70%) and carbon content in this phase. The resulting duplex ferritic/martensitic microstructures are illustrated in Fig. 2. Essentially, air cooling from 1100°C results in a fine

Table I. Composition in Wt Pct of AISI 1008 and 1015 Mild Steels

Steel	C	Mn	Si	P	S	Al	Cr
AISI 1008	0.08	0.26	0.20	0.01	0.01	-	-
AISI 1015	0.14	0.77	0.21	0.02	0.01	0.04	0.02

distribution of hypo-eutectoid ferrite plus pearlite which, on annealing in the ($\alpha + \gamma$) region, causes austenite to nucleate on carbide/ferrite interfaces, giving a fine globular martensite (α') on ferrite grain boundaries. The ferritic phase, however, is virtually continuous in encapsulating the martensite, and has an average grain size in all structures between 50 and 90 μm. Results on the duplex microstructures were compared with conventionally normalized structures (containing 0% martensite), obtained by air cooling from 1100°C (1 h). Quantitative metallography and mechanical property data are listed in Tables II and III, respectively.

To minimize residual stresses, test specimens were machined following the final ice-brine quench (a surface layer of at least 3 mm was removed from all faces and edges), and then were stress-relieved for 2 h at 200°C. As subsequent fatigue surface showed little influence of crack front curvature, such procedures were considered to be effective.

Fatigue crack growth tests on long ($\geq$ 20 mm) cracks were performed using 12.7 mm thick compact C(T) specimens (L-T orientation), tested under load control in electroservo-hydraulic

Table II. Microstructural Characteristics of Intercritically Annealed AISI 1008 and 1015 Dual-Phase Steels

Steel	Annealing Temp. (°C)	Martensite Vol. Fraction (pct)	Carbon Content in Martensite (pct)
AISI 1008	793	26	0.35
	829	46	0.19
	850	67	0.14
AISI 1015	760	31	0.53
	808	53	0.28
	824	67	0.22

Table III. Ambient Temperature Mechanical Properties of Intercritically Annealed AISI 1008 and 1015 Mild Steels

Steel	Martensite Vol. Fraction (pct)	Yield Strength (0.2%offset) (MPa)	U.T.S. (MPa)	Redn. in Area (pct)	Elongation (14 mm gauge) (pct)
AISI 1008	26	346	477	79	24
	46	360	479	73	28
	67	410	560	72	24
(normalized)	0	203	349	74	32
AISI 1015	31	392	555	66	26
	53	427	602	73	28
	67	433	603	72	22
(normalized)	0	265	422	70	31

testing machines at a frequency of 50 Hz (sine wave). Tests were conducted, over a range of growth rates from 10^{-11} to 10^{-6} m/cycle, in controlled room air (22°C, 45% relative humidity), with a load

ratio R of 0.05. Fatigue threshold stress intensity ranges (ΔK_{TH}), defined at a maximum growth rate of 10^{-11} m/cycle, were approached using manual load shedding procedures,* with crack lengths

*Near-threshold growth rates were determined under decreasing ΔK conditions, using a step-wise decrease in ΔK of less than 5 pct at each step. At each load level, the crack was propagated a distance of at least 3 times the computed maximum plastic zone size formed at the previous load level. Following definition of the threshold, growth rates were additionally measured under increasing ΔK conditions.

continuously monitored using d.c. electrical potential methods. Simultaneous measurement of crack closure was achieved using the back-face strain technique (1,16). With such a technique, the closure stress intensity (K_{cl}) is defined during unloading at first contact of the fracture surfaces from the load corresponding to the initial deviation from linearity of the elastic compliance curve, derived from a strain gauge mounted on the back face of the specimen (1).

Fatigue crack growth tests on microstructurally-small ($\sim$ 10 to 1000 μm) cracks were performed using small 6.4 mm thick four-point bend specimens (with maximum bending stress at surface less than 0.95 of the yield stress), cycled under identical load ratio, frequency and environmental conditions as the C(T) samples. The initiation and early growth of naturally-occurring surface cracks in these specimens was monitored by periodic replication of the top surface using cellulose replicas. Replicas were subsequently gold

coated to permit better resolution. Due to crack meandering, surface crack length was measured as the projected length normal to the tensile bending stress. Stress intensities were computed from the Newman and Raju (17) solution for semi-elliptical surface flaws. An a/c (half surface length to crack depth ratio) of 1 was assumed, based on studies of crack geometry by serial sectioning. The use of K was deemed to be appropriate as computed cyclic plastic zone sizes remained small compared to crack length, i.e., in the range 0.7 to 20 μm for crack sizes of 10 to 1000 μm, respectively.

Fatigue crack initiation properties were evaluated from (smooth bar) fatigue limit data, determined from constant amplitude S/N curves. Tests were performed on 6.4 mm diameter unnotched tensile specimens, using a closed loop resonant testing machine, operating at a frequency of 110 Hz and a load ratio of 0.05. All specimens were manually polished along the longitudinal axis (stress axis) and electropolished in acetic chromium trioxide solution to eliminate tangential scratches. The fatigue limit was defined as the highest stress amplitude which did not cause failure of the specimen within 10^8 cycles.*

---

*Subsequent scanning electron microscopy often revealed that crack nucleation had occurred in the ferrite with the crack arresting in the martensite.

Crack path morphologies were examined on metallographic sections, taken at the specimen center thickness perpendicular to the

fracture surface (on cracks previously impregnated with epoxy). Measurements were made of the fraction of cracking in the martensite and the degree of fracture surface roughness. The latter was assessed in terms of the mean angle of crack deflection from the plane of maximum tensile stress, and the lineal surface roughness, measured as the ratio of the total length of crack to the projected length along the plane of maximum tensile stress. The extent of crack surface corrosion deposits was estimated using scanning Auger Spectroscopy with an Ar^+ sputtering rate of 1000 Å/min. The excess oxide thickness was computed using a tantalum oxide standard, assuming a Pilling-Bedworth ratio of ∿2.0 for iron.*

*Since one unit of iron oxidizes to roughly two volumes of oxide (e.g., Pilling-Bedworth ratio for Fe_2O_3 = 2.13), the oxide thickness measurements on one half of the fracture surface represent approximately the total excess material, assuming only thickness-direction growth and equal thicknesses on each crack face (10).

III. RESULTS AND DISCUSSION

A. Long Crack Behavior

Growth Rates: The variation in long crack fatigue crack propagation rates, da/dN, with the nominal stress intensity range, ΔK, for the AISI 1008 and 1015 steels is shown in Fig. 3. Results for the duplex microstructures are compared with those for normalized structures, and in both steels show higher ΔK_{TH} values (Table IV) and progressively lower growth rates as the threshold is approached.

Table IV. Fatigue Threshold Data in Intercritically Annealed AISI 1008 and 1015 Dual Phase Steels

Steel	Martensite Vol. Fract.	Growth Threshold ΔK_{TH}		Initiation Threshold Fatigue Limit, $\Delta\sigma_{TH}/2$		
		Nominal	Effective	R=0.5	R=-1*	$\frac{\Delta\sigma_{TH}}{2}/UTS$
	(pct)	($MPa\sqrt{m}$)		(MPa)		
AISI 1008	26	20.1	2.6	145	219	0.46
	46	12.9	6.0	169	277	0.58
	67	13.3	4.6	147	206	0.37
(normalized)	0	9.2	3.0	-	-	-
AISI 1015	31	15.5	6.1	186	283	0.51
	53	18.1	4.0	174	226	0.38
	67	14.7	3.7	190	291	0.48
(normalized)	0	12.3	4.4	-	-	-

*Computed from R = 0.05 value using the Goodman relationship (24).

Behavior, however, is dependent on the volume fraction of martensite. The dual-phase 26 pct martensite structure in AISI 1008 has the lowest growth rates over the entire range (from threshold to near instability), with a threshold ΔK_{TH} of over 20 $MPa\sqrt{m}$ (Fig. 3a). This is to be compared with a value of 9.2 $MPa\sqrt{m}$ in normalized AISI 1008, and represents a 120 pct increase. Growth rate behavior in the dual-phase 46 and 67 pct martensite structures is less spectacular, but thresholds are still 40 to 45 pct higher than in the normalized steel. A similar influence of duplex microstructure is apparent in AISI 1015 steel (Fig. 3b), although differences are not as large; the dual-phase 53 pct martensite structure shows the lowest growth rates,

with a ΔK_{TH} value of over 18 MPa$\sqrt{m}$, 47 pct higher than in the normalized structure.*

---

*It is important to note here that, contrary to behavior usually reported for steels (18), in both AISI 1008 and 1015 steels, the duplex microstructures show higher thresholds than the normalized structures, despite having yield strengths which are 48 to 102 pct higher. Based on previously reported results (19-23), this appears to be a characteristic of dual-phase steels.

Crack Closure: Corresponding back-face measurements of crack closure, plotted as the effective load ratio, K_{cl}/K_{max}, as a function of ΔK, are shown in Fig. 4, and indicate very high levels of crack tip shielding in the dual-phase structures. Characteristic of wedge shielding behavior (10), closure is enhanced as the CTOD decreases, i.e., with progressively decreasing ΔK, with the K_{cl} values at threshold approaching as much as 90 pct of K_{max}. For both steels, the ranking of structures in terms of highest closure levels (at fixed ΔK) exactly coincides with their ranking in terms of lowest growth rates and highest thresholds. In particular, closure levels in the duplex 26 pct martensite structure in AISI 1008 were exceptionally high and exceeded K_{cl}/K_{max} values of 0.5 at ΔK levels as high as 30 MPa$\sqrt{m}$ (Fig. 4b), consistent with the very low growth rate behavior and high threshold shown by this microstructure. In fact, the computed ΔK_{eff} at the threshold in this structure was a mere 2.6 MPa$\sqrt{m}$, i.e., a factor of 8 times smaller than the nominal ΔK_{TH}. Moreover, compared to the wide variation in nominal thresholds,

effective thresholds (after allowing for closure) varied only from 2.6 to 6.0 MPa$\sqrt{m}$ in the two steels. Corresponding levels of crack closure in the normalized steels were always lower (at fixed ΔK) than corresponding levels in the duplex structures; effective thresholds were approximately 4 MPa$\sqrt{m}$.

Fracture Surface and Crack Path Morphology: SEM fractographs of fatigue surfaces at low (near ΔK_{TH}) and high (25 to 30 MPa$\sqrt{m}$) ΔK levels are shown in Fig. 5 for the dual-phase structures in AISI 1008 with highest and lowest thresholds, i.e., the 26 and 46 pct martensite structures, respectively. Corresponding crack path profiles are shown in Fig. 6, and are quantitatively analyzed in Table V. At low ΔK, fatigue surfaces in the 26 pct martensite structure exhibited a rough "hill and valley" type fracture, with an associated zig-zag path primarily through the ferrite (Figs. 5a,6a). Such fractures show high lineal roughness and high crack deflection angles (Table V), characteristic of extensive crack closure induced by asperity wedging (roughness-induced closure). In contrast, surfaces in the 46 pct martensite structure resembled quasi-cleavage, were relatively planar (i.e., low crack deflection angles), and involved crack growth predominately in the martensite (Figs. 5b,6b). At high ΔK, the crack path in both structures favored the ferrite phase and showed evidence of ductile striations (e.g., Fig. 5d). Fracture surfaces in the 26 pct martensite structure were similar to those at low ΔK (Fig. 5c), with the crack path showing marked crack

Table V. Crack Path Morphology Measurements in AISI 1008 Steel

Structure	Low ΔK (near ΔK_{TH})			High ΔK (25-30 MPa$\sqrt{m}$)		
	Lineal Roughness	Mean Angular Deviation (deg)	Crack Path in α' (pct)	Lineal Roughness	Mean Angular Deviation (deg)	Crack Path in α' (pct)
26% α'	1.25	55^o - 60^o	15	1.08	35^o - 40^o	26
46% α'	1.17	20^o - 25^o	74	1.17	20^o - 25^o	41

deflection on encountering the martensite phase (Fig. 6c), whereas in the 46 pct martensite structure they remained relatively planar (Fig. 6d).

Fracture surfaces in AISI 1015 steel displayed the same general characteristics as in AISI 1008. However, the 31 pct martensite structure shows extensive cleavage fracture in the ferrite during crack growth at high ΔK (Fig. 7).

Near-threshold fracture surfaces were also characterized by extensive fretting corrosion deposits. Auger spectroscopy measurements of the debris indicated similar thickness profiles in both 26 and 46 pct martensite structures, i.e., a peak in excess oxide thickness ($\sim$0.8 μm) close to ΔK_{TH}, and a thickness comparable with the natural limiting oxide thickness ($<$0.05 μm) at high growth rates. These results, together with the lineal roughness data, are plotted as a function of da/dN and crack length in Fig. 8.

Comparison of the peak excess oxide thicknesses and the mean fracture surface asperity sizes in AISI 1008 with computed crack tip opening displacements at the threshold (Table VI) gives a clear indication of the sources of crack tip shielding in these microstructures. First, the increased mean crack deflection angle and lineal roughness in the 26 pct martensite structure suggests enhanced shielding by crack deflection and meandering, respectively, compared to the 46 pct martensite structure. Such shielding can remain effective at higher growth rates (1), although in the present case its effect will be diminished by less deflection at high ΔK. Second, the tortuosity in crack path, and consequently much larger asperity sizes, will promote progressively higher levels of roughness-induced crack closure in the 26 pct martensite structure as ΔK is reduced (Fig. 9), consistent with the measured K_{cl} data (Fig. 4a). Peak oxide thicknesses are also comparable with cyclic CTOD levels close to ΔK_{TH}, indicating additional wedge shielding from

Table VI. Mean Asperity, Oxide Debris and CTOD's Sizes Associated with ΔK_{TH} in Dual-Phase AISI 1008 Steel

Structure	Threshold		CTOD*		Mean Asperity Size	Excess Oxide Thickness
	ΔK_{TH}	ΔK_{eff}	max	cyclic		
	($MPa\sqrt{m}$)		(μm)		(μm)	(μm)
26% α'	20.1	2.6	3.0	1.4	1.8	0.80
46% α'	12.9	6.0	1.2	0.5	0.2	0.81

oxide-induced closure. However, since oxide thicknesses are only significant close to ΔK_{TH} (Fig. 8), contributions from this mechanism will be specific to very low growth rates.

B. Crack Initiation (S/N) Behavior

S/N curves for the dual-phase structures in AISI 1008 and 1015 are shown in Fig. 10. Values of the unnotched 10^8 cycle fatigue limit ($\Delta\sigma_{TH}/2$), representing a threshold for crack initiation (26,27), are listed in Table IV. It is pertinent to note that the 46 pct martensite structure in AISI 1008 and the 67 pct martensite structure in AISI 1015 show the **highest** fatigue limits (i.e., $\Delta\sigma_{TH}/2 \approx 0.5$ and 0.6 UTS, respectively), yet these structures show the **lowest** values of ΔK_{TH}. In fact, **the ranking of the duplex structures in each steel with respect to crack initiation thresholds is exactly the opposite that for (long) crack propagation thresholds.** This is illustrated in Fig. 11 for the AISI 1008 steel, and is characteristic of crack growth behavior dominated by crack tip shielding. Unnotched fatigue limits effectively characterize the intrinsic resistance to fatigue, since without major cracks, shielding cannot be effective. Long crack growth thresholds (at low R), conversely, are controlled far more by extrinsic shielding processes, which rarely have the same dependence on microstructure. However, by subtracting out the extrinsic contribution from closure, crack initiation and crack growth thresholds can be seen to show the same trends with microstructure (Fig. 11).

C. Small Crack Behavior

Results of the small crack tests performed on the dual-phase 26 and 46 pct martensite structures in AISI 1008 are plotted in Fig. 12. Considerable scatter is apparent in crack growth rates, characteristic of naturally-occurring microstructurally-small cracks which undergo frequent impedence at grain boundaries and at ferrite/martensite interfaces. For example, cracks tended to undergo marked changes in direction to avoid martensitic regions (e.g., areas marked A in Fig. 13), or when blunted and locally arrested at ferrite grain boundaries, as shown by the heavy slip-band activity in areas marked B in these figures. However, it is clear that the small cracks propagate at stress intensity ranges as low as 1.5 MPa$\sqrt{m}$, well below the long crack thresholds. Moreover, they show indications of progressively decreasing growth rates during their initial growth stage ($a \lesssim 20$ μm), characteristic of small crack behavior (1,28-34). Such decelerations have been attributed to crack shape evolution during initial growth (30,31), where the crack depth grows faster than on the surface until the equilibrium crack configuration is reached, and to the development of crack tip shielding with the generation of a crack wake (1,29,30).

Similar to the contrasting effects of duplex microstructure on long crack thresholds and fatigue limits, small cracks appear to grow faster (at a given ΔK) in the 26 pct martensite structure, whereas exactly the reverse is true for long crack growth. Again, this is characteristic of fatigue behavior controlled by the mutual

competition of extrinsic and intrinsic processes. Crack tip shielding, via mechanisms such as roughness-induced crack closure, will be relatively ineffective for small cracks by virtue of their restricted wake, such that behavior, in contrast to long cracks, will be more influenced by intrinsic mechanisms. This distinction between the behavior of long and small cracks in terms of a differing influence of crack closure can be appreciated in Fig. 14, where the small crack growth rates are compared with long crack growth rates plotted as a function of ΔK_{eff}. It is apparent, at least in the 26 pct martensite structure, that once long crack data are corrected for closure, good correspondence is achieved between long and small crack results. (The same appears to be true for the 46 pct martensite structure, although the long cracks arrest before an overlap of data occurs).

Although care must be exercised in interpreting growth rate data plotted as a function of ΔK_{eff}, due to experimental uncertainities in the measurement of K_{cl}, the present results do show that small cracks, even after allowing for closure, **can propagate below the long crack (ΔK_{eff}) threshold** (Fig. 14). Similar behavior has been reported for microstructurally-small cracks in aluminum alloys (1,28,32), and indicates that shielding via crack closure does not completely rationalize the enhanced growth rates of small flaws (although it clearly provides a major contribution). The nature of the other contributing mechanisms is currently uncertain (1,28), although naturally-occurring small cracks, unlike pre-existing long

cracks, tend to nucleate at the "soft spots" in the microstructure and grow into the most favorably orientated grains (33). Furthermore, in situ measurements on microstructurally-small cracks in aluminum alloys (28,34) have indicated higher crack tip cyclic plastic strains, compared to long cracks at the same ΔK.

IV. INTRINSIC VS. EXTRINSIC TOUGHENING

The intent of this study has been to show how composite microstructures in plain carbon steels can induce unusally good fatigue properties, through the enhancement of both intrinsic and extrinsic "toughening" mechanisms. In fact, with respect to long crack growth behavior, the specific properties of the dual-phase 26 pct martensite microstructure in AISI 1008 steel represent the highest fatigue threshold reported to date for a metallic alloy, namely a ΔK_{TH} value above 20 MPa$\sqrt{m}$ (Fig. 15). In Fig. 15, it is also apparent that a unique characteristic of duplex microstructures is that their superior crack growth properties can be obtained without compromise in strength.

The outstanding long crack growth properties in dual-phase ferrous microstructures (see also refs. 19-23) are clearly derived extrinsically through the development of a meandering crack path, i.e., from crack tip shielding resulting from reductions in local stress intensity primarily from crack deflection and resulting roughness-induced crack closure from asperity wedging, with an additional contribution from oxide-induced closure. The relative

contributions from deflection and closure are estimated by comparing the normalized structure in AISI 1008, where the crack path is predominantly linear, with the dual-phase 26 and 46 pct martensite structures, which exhibit lineal roughnesses of approximately 1.2 and 1.3, respectively. Experimental growth rate data for these two structures are first corrected for closure by plotting as a function of ΔK_{eff}, using the back-face strain measurements of K_{cl} (Fig. 16a). Next, predictions of the effect of crack deflection are applied to the nominally linear crack path of the normalized structure (Fig. 16b), using two-dimensional linear elastic models (6). Here, by considering repeated crack segments involving a deflection angle θ, a deflected distance D, and an undeflected distance S, the effective stress intensity range, $(\Delta K)_D$, and growth rate, $(da/dN)_D$, of an idealized deflected crack are given by (6):

$$(\Delta K)_D = \left[\frac{D \cos^2(\theta/2) + S}{D + S}\right] (\Delta K)_L \quad , \qquad (1a)$$

$$(da/dN)_D = \left[\frac{D \cos\theta + S}{D + S}\right] (da/dN)_L \quad , \qquad (1b)$$

where $(\Delta K)_L$ and $(da/dN)_L$ are the nominal stress intensity range and growth rate of the linear undeflected Mode I crack, respectively. Quantifying the degree of deflection is complicated by the non-uniform nature of crack path meandering. However, selecting extreme values of the angle of tilt θ to vary between 0 and 75^o, with D/(D + S) between 0 and 0.75, predictions of the effect of deflection alone

on crack growth behavior can be obtained. The results in Fig. 16b suggest that the contribution to shielding from deflection alone remains relatively small compared to that due to crack closure. However, it is important to note that, while deflection is not a major extrinsic "toughening" mechanism per se, its occurrence generally promotes other, more potent, shielding mechanisms, such as roughness-induced crack closure during fatigue or crack bridging in ceramics (35).

With reference to the AISI 1008 steel, although the duplex 26 pct martensite structure displays optimum (long) crack growth properties due principally to the extrinsic mechanisms of crack deflection and closure, in terms of intrinsic fatigue resistance, the 46 pct martensite structure apparently is superior. This is shown by its higher fatigue limit (Fig. 10), marginally slower small crack growth rates (Fig. 11), lower long crack growth rates (as a function of ΔK_{eff}) and higher long crack effective threshold (once closure has been removed) (Fig. 14). Enhanced extrinsic "toughening" in the dual phase 26 pct martensite structure can be attributed to the crack preferentially following the softer phase (the ferrite is continuous in this structure) and to crack deflection at ferritic/martensitic interfaces, both of which induce the tortuous crack path.* In the 46

*The incorporation of a continuous soft phase is also used in the toughening of ceramic composites. For example, in tungsten carbide, the addition of cobalt as a continuous soft phase induces a tortuous crack path in the metal, which imparts significant extrinsic toughening from deflection and associated crack bridging.

pct martensite structure, where the near-threshold crack path favors the martensite, crack extension is intrinsically slower, presumably due to the higher strength of this phase. This is consistent with studies (26,27) which have identified the fatigue limit in dual-phase steels with the presence of microcracks, which initiate in the ferrite yet arrest in the martensite. However, higher volume fractions of martensite do not appear to offer further advantages (20).

Finally, the fatigue behavior of dual-phase steels is an excellent example of extrinsic "toughening" (2). The mechanisms of such toughening are largely dependent on such variables as crack size, geometry, CTOD, etc., and thus, unlike intrinsic toughening, are not a property of the material. Where this approach can be utilized, i.e., with materials of low intrinsic toughness or where crack growth occurs at low stress intensities, the very potent effect of crack tip shielding mechanisms in inducing superior long crack growth properties must be tempered with significantly enhanced small crack effects, and contrasting effects of microstructure on crack initiation and crack growth. Similar behavior is to be expected in other microstructures which show significant crack path meandering. This is apparent in other dual-phase microstructures, such as duplex α/β titanium alloys (36), or where crack deflection can be induced crystallographically. An excellent example of the latter case is in coherent particle hardened materials showing marked planar slip behavior, such as aluminum-lithium alloys, which, compared to

traditional aluminum alloys, display superior long fatigue crack growth properties (37-40), yet very high small crack growth rates (32,40).

V. CONCLUSIONS

Based on an investigation into the role of crack tip shielding in influencing the initiation and growth of long ($\geq$ 20 mm) and naturally-occurring small (10 to 1000 μm) fatigue cracks in composite ferritic-martensitic microstructures in AISI 1008 and 1015 mild steels, the following conclusions can be made:

1. Dual-phase microstructures in AISI 1008, containing between 26 and 67 pct martensite, were found to have superior long fatigue crack growth properties (and higher yield strengths) compared to conventional normalized structures, with fatigue threshold ΔK_{TH} values (at R = 0.05) at least 40 pct higher. The 26 pct martensite structure displayed a (nominal) threshold of ΔK_{TH} = 20.1 MPa$\sqrt{m}$, representing the highest threshold reported to date for a metallic material.
2. Long crack growth results for dual-phase microstructures in AISI 1015, containing between 31 and 67 pct martensite, were similar, with thresholds between 20 and 47 pct higher (with higher yield strengths), compared to the normalized structure. Optimum properties were achieved with the 53 pct martensite structure, which displayed a (nominal) threshold of ΔK_{TH} = 18.1 MPa$\sqrt{m}$.

3. The excellent long crack growth properties in duplex microstructures were found to be consistent with very high measured levels of crack closure (i.e., K_{cl} values approaching 0.9 K_{max} as ΔK_{TH} was approached). At fixed ΔK, the ranking of the microstructures in terms of lowest growth rates was identical to that in terms of highest closure levels.

4. Such high measured levels of crack closure in the dual-phase microstructures were consistent with an increased tortuosity of crack path. Such tortuosity, which was induced by preferential crack paths in the softer ferrite, and/or from marked crack deflection at ferrite/ferrite and ferrite/martensite interfaces, was considered to result in a significant contribution to crack tip shielding, from both crack deflection and roughness-induced crack closure. Using simple modeling concepts, the contribution to shielding from closure was estimated to be the more significant.

5. From smooth bar S/N tests on the duplex microstructures, fatigue limits (representing an effective threshold stress for crack initiation) were found to be in the range of 0.4 to 0.6 of the UTS. In both steels, the ranking of the microstructures with highest resistance to crack initiation was exactly the opposite to that for crack growth (based on da/dN vs. ΔK data). When analyzed in terms of ΔK_{eff} (after correcting for closure), however, the rankings of the microstructures in terms of crack initiation and growth became identical.

6. In the duplex 26 and 46 pct martensite structures in AISI 1008, small cracks were observed to propagate at stress intensity ranges as low as 1.5 MPa$\sqrt{m}$, almost an order of magnitude lower than the (nominal) long crack ΔK_{TH} thresholds. However, when plotted in terms of ΔK_{eff} (after correcting for closure), close correspondence was achieved between long and small crack growth rate behavior (except below $\Delta K_{TH,eff}$). No evidence of an intrinsic threshold for small crack growth was apparent. Despite the fact that long crack growth rates were significantly slower (at fixed ΔK) in the 26 pct martensite structure, small crack growth rates were marginally faster.

7. The contrasting effects of duplex microstructure on resistance to long crack growth, compared to crack initiation and small crack growth, are characteristic of behavior governed by the mutual competition of extrinsic and intrinsic "toughening" mechanisms. The most potent crack tip shielding, which impedes long crack growth, is achieved from crack tortuosity, via preferential crack paths in the ferrite. However, as shielding is of minimal significance for cracks of limited wake, optimum crack initiation and small crack resistance is apparent where cracks primarily intersect the martensite.

ACKNOWLEDGMENTS

This work was supported by the Director, Office of Energy Research, Office of Basic Energy Sciences, Materials Science Division of U.S. Department of Energy under Contract No. DE-AC03-76SF00098. Thanks are due to Professor Gareth Thomas for helpful discussions, to Dr. Weikang Yu for experimental assistance, and to Madeleine Penton for help in preparing the manuscript.

REFERENCES

1. R. O. Ritchie and W. Yu, in Small Fatigue Cracks, R. O. Ritchie and J. Lankford, eds., TMS-AIME, Warrendale, PA, 1986, pp. 167-89.

2. R. O. Ritchie and R. M. Cannon, Lawrence Berkeley Laboratory Report No. LBL-20656, University of California, Berkeley, Dec. 1985.

3. R. M. McMeeking and A. G. Evans, J. Amer. Cer. Soc., vol. 65, 1982, pp. 242-6.

4. A. G. Evans and K. T. Faber, J. Amer. Cer. Soc., vol. 67, 1984, pp. 255-60.

5. D. B. Marshall, B. N. Cox, and A. G. Evans, Acta. Metall., vol. 33, 1985, pp. 2013-21.

6. S. Suresh, Metall. Trans. A, vol. 14A, 1983, pp. 2375-85.

7. S. Suresh and R. O. Ritchie, in Fatigue Crack Growth Threshold Concepts, D. L. Davidson and S. Suresh, eds., TMS-AIME, Warrendale, PA, 1984, pp. 227-61.

8. R. O. Ritchie, S. Suresh, and C. M. Moss, J. Eng. Matls. Tech., Trans. ASME, Ser. H, vol. 102, 1980, pp. 293-9.

9. A. T. Stewart, Eng. Fract. Mech., vol. 13, 1980, pp. 463-78.

10. S. Suresh, G. F. Zamiski, and R. O. Ritchie, Metall. Trans. A, vol. 12A, 1981, pp. 1435-43.

11. N. Walker and C. J. Beevers, Fat. Eng. Mat. Struct., vol. 1, 1979, pp. 135-48.

12. K. Minakawa and A. J. McEvily, Scripta Met., vol. 6, 1981, pp. 633-6.

13. S. Suresh and R. O. Ritchie, Metall. Trans. A, vol 13A, 1982, pp. 1627-31.

14. J.-L. Tzou, C. H. Hsueh, A. G. Evans, and R. O. Ritchie, Acta Metall. vol. 33, 1985, pp. 117-27.

15. W. Elber, Eng. Fract. Mech., vol. 2, 1970, pp. 37-45.

16. W. F. Deans and C. E. Richards, J. Test. Eval., vol. 7, 1979, p. 147.

17. J. C. Newman, Jr. and I. S. Raju, Eng. Fract. Mech., vol. 15, 1981, pp. 185-92.

18. R. O. Ritchie, Int. Metals Reviews, vol. 20, 1979, pp. 205-30.

19. H. Suzuki and A. J. McEvily, Metall. Trans. A, vol. 10A, 1979, p. 475.

20. K. Minakawa, Y. Matsuo, and A. J. McEvily, Metall. Trans. A, vol. 13A, 1982, p. 439.

21. J. A. Wasynczuk, R. O. Ritchie, and G. Thomas, Mat. Sci. Engr., vol. 62, 1984, pp. 79-92.

22. V. B. Dutta, S. Suresh, and R. O. Ritchie, Metall. Trans. A, vol. 15A, 1984, pp. 1193-207.

23. J.-L. Tzou and R. O. Ritchie, Scripta Met., vol. 19, 1985, pp. 751-5.

24. M. R. Mitchell, in Fatigue and Microstructure, American Society for Metals, Metals Park, OH, 1979, pp. 385-466.

25. C. F. Shih, J. Mech. Phys. Solids, vol. 21, 1981, p. 305.

26. T. Kunio and K. Yamata, in Fatigue Mechanisms, ASTM STP 675, J. T. Fong, ed., American Society for Testing and Materials, Philadelphia, PA, 1979, pp. 342-61.

27. T. Konio, M. Shimizu, K. Yamata, and H. Nakabayashi, in Fatigue Thresholds, J. Bäcklund, A. F. Blom, and C. J. Beevers, eds., EMAS Ltd., Warley, U.K., vol. 1, 1982, pp. 409-22.

28. J. Lankford, Fat. Fract. Eng. Mat. Struct., vol. 8, 1985, pp. 161-75.

29. S. Suresh and R. O. Ritchie, Int. Metals Reviews, vol. 29, 1984, pp. 445-76.

30. A. Pineau, in Small Fatigue Cracks, R. O. Ritchie and J. Lankford, eds., TMS-AIME, Warrendale, PA, 1986, pp. 191-212.

31. L. Wagner, J. K. Gregory, A. Gysler, and G. Lütjering, in Small Fatigue Cracks, R. O. Ritchie and J. Lankford, eds., TMS-AIME, Warrendale, PA, 1986, pp. 117-28.

32. K. T. Venkateswara Rao, W. Yu, and R. O. Ritchie, Scripta Met., vol. 20, 1986, pp. 1459-65.

33. R. O. Ritchie and J. Lankford, Mater. Sci. Eng., vol. 84, 1986, pp. 11-6.

34. J. Lankford and D. L. Davidson, in Small Fatigue Cracks, R. O. Ritchie and J. Lankford, eds., TMS-AIME, Warrendale, PA, 1986, pp. 51-72.

35. R. Steinbrech, R. Knehans, and W. Schaarwächter, J. Mat. Sci., vol. 18, 1983, pp. 265-70.

36. J. M. Larsen, T. Nicholas, A. W. Thompson, and J. C. Williams, in Small Fatigue Cracks, R. O. Ritchie and J. Lankford, eds., TMS-AIME, Warrendale, PA, 1986, pp. 499-512.

37. J. Petit, S. Suresh, A. K. Vasudévan, and R. C. Malcolm, in Aluminium-Lithium Alloys III, C. Baker, P. J. Gregson, S. J. Harris, and C. J. Peel, eds., Institute of Metals, London, U.K., 1986, pp. 257-62.

38. K. V. Jata and E. A. Starke, Jr., Metall. Trans. A, vol. 17A, 1986, pp. 1011-26.

39. W. Yu and R. O. Ritchie, J. Eng. Matls. Tech., Trans. ASME, Ser. H, vol. 109, 1987, pp. 81-5

40. K. T. Venkateswaro Rao, W. Yu, and R. O. Ritchie, Metall. Trans. A, vol. 18A, 1987, in review.

EXTRINSIC TOUGHENING MECHANISMS

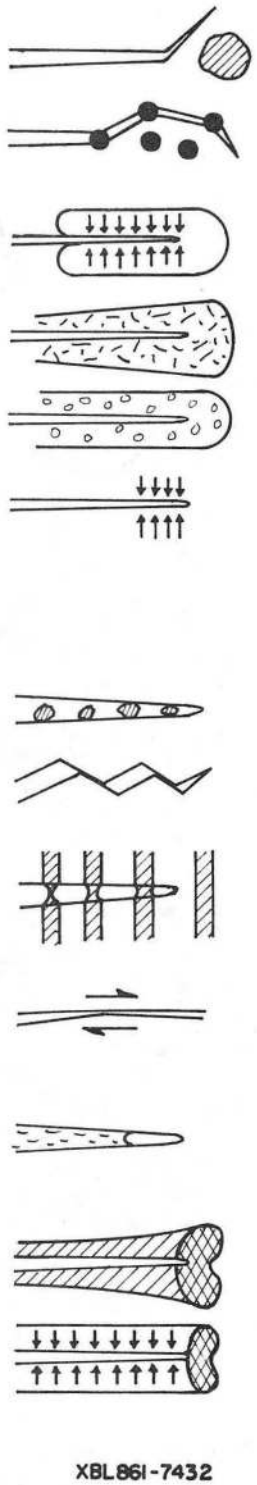

Fig. 1. Schematic representation of the classes and mechanisms of crack tip shielding (after refs. 1,2).

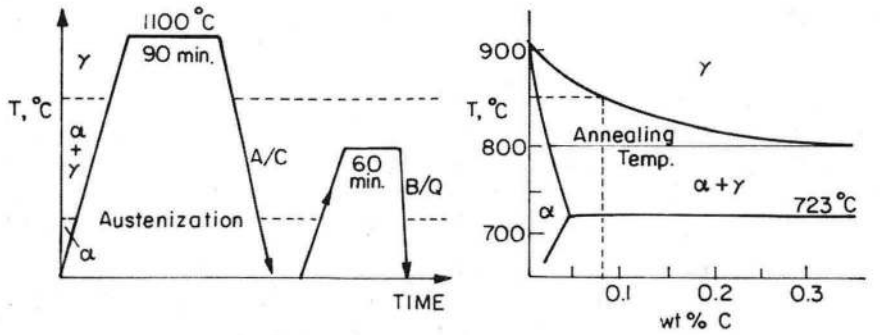

(a) Intercritical Annealing Cycle

AISI 1008 STEEL

100 μm

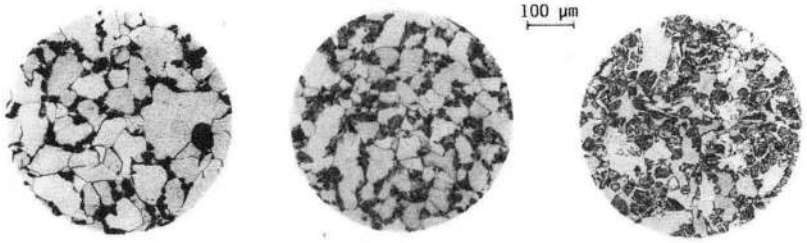

Anneal : 793 °C	829 °C	850 °C
Martensite : 26 %	46 %	67 %
C in α' : 0.35 %	0.19 %	0.14 %

AISI 1015 STEEL

Anneal: 760 °C	808 °C	824 °C
Martensite: 31 %	53 %	67 %
C in α': 0.53 %	0.28 %	0.22 %

(b) Ferrite/Martensite Duplex Microstructures

XBB 862-1023A

Fig. 2. Intercritical heat treatment sequences and resulting duplex ferritic/martensitic microstructures in AISI 1008 and 1015 mild steels. (Microstructures etched in 2 pct nital).

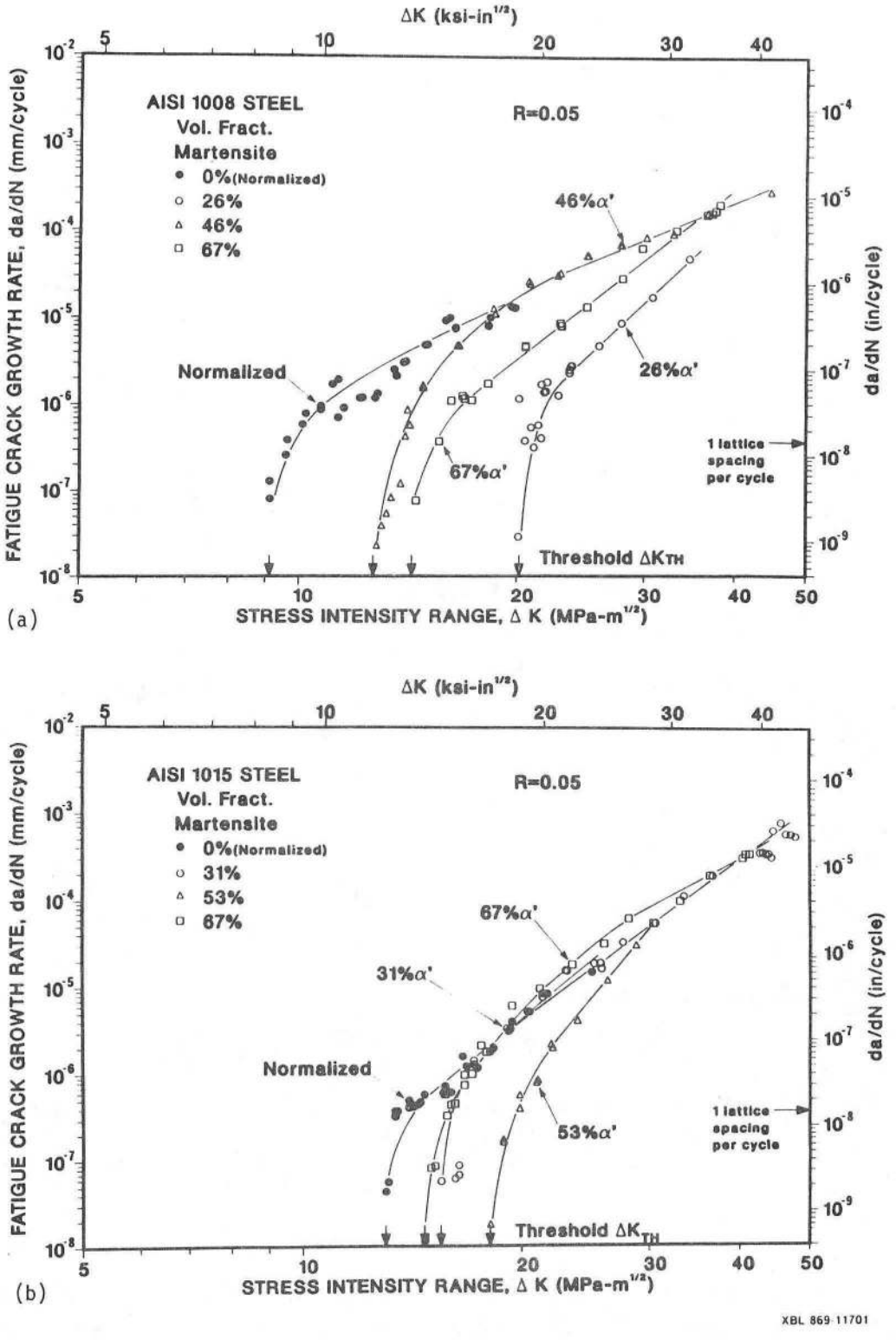

Fig. 3. Comparison of fatigue (long) crack propagation rates (da/dN), as a function of the nominal stress intensity range (ΔK), in normalized and duplex ferritic/martensitic microstructures in a) AISI 1008 and b) AISI 1015 steels.

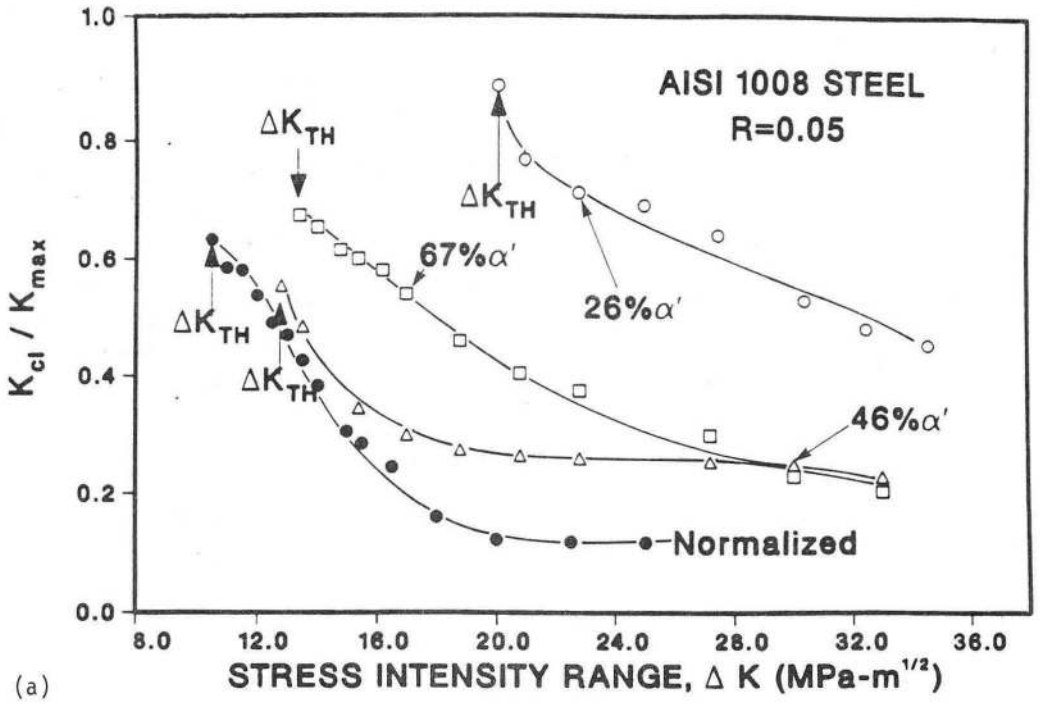

(a)

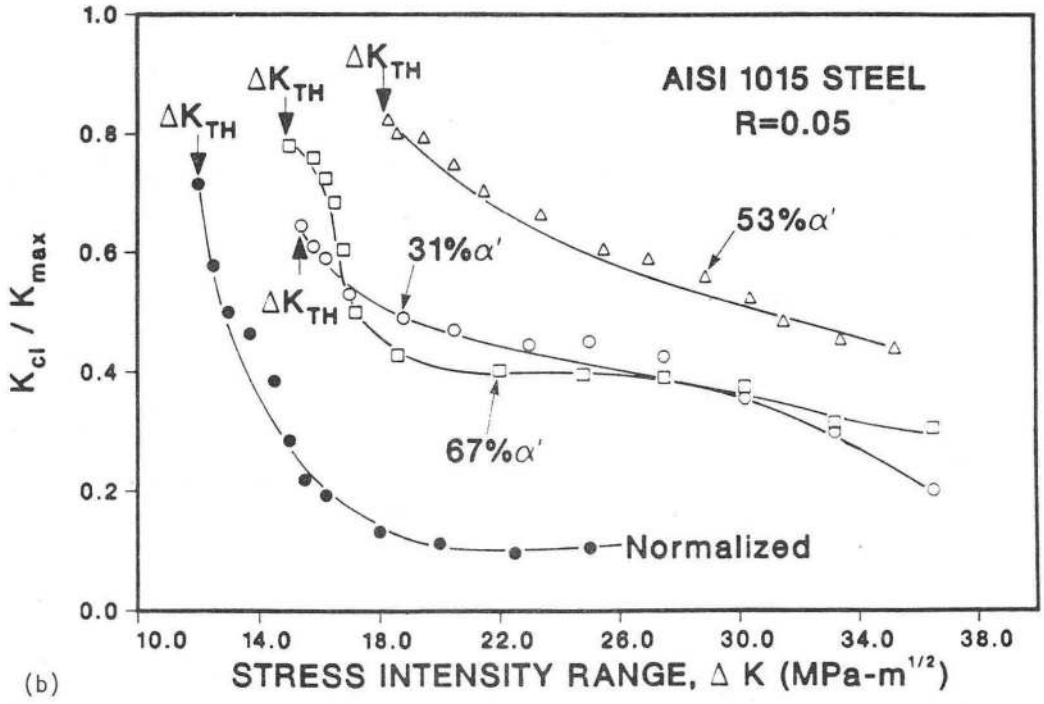

(b)

XBL 869-11700

Fig. 4. Experimental back-face strain measurements of crack closure corresponding to long crack growth rates in Figs. 3 and 4, showing variation of closure stress intensity (K_{cl}), normalized by the maximum stress intensity (K_{max}), as a function of stress intensity range (ΔK) for a) AISI 1008 and b) AISI 1015 steels. Note how closure is progressively enhanced with decreasing ΔK, approaching K_{cl}/K_{max} levels of 0.9.

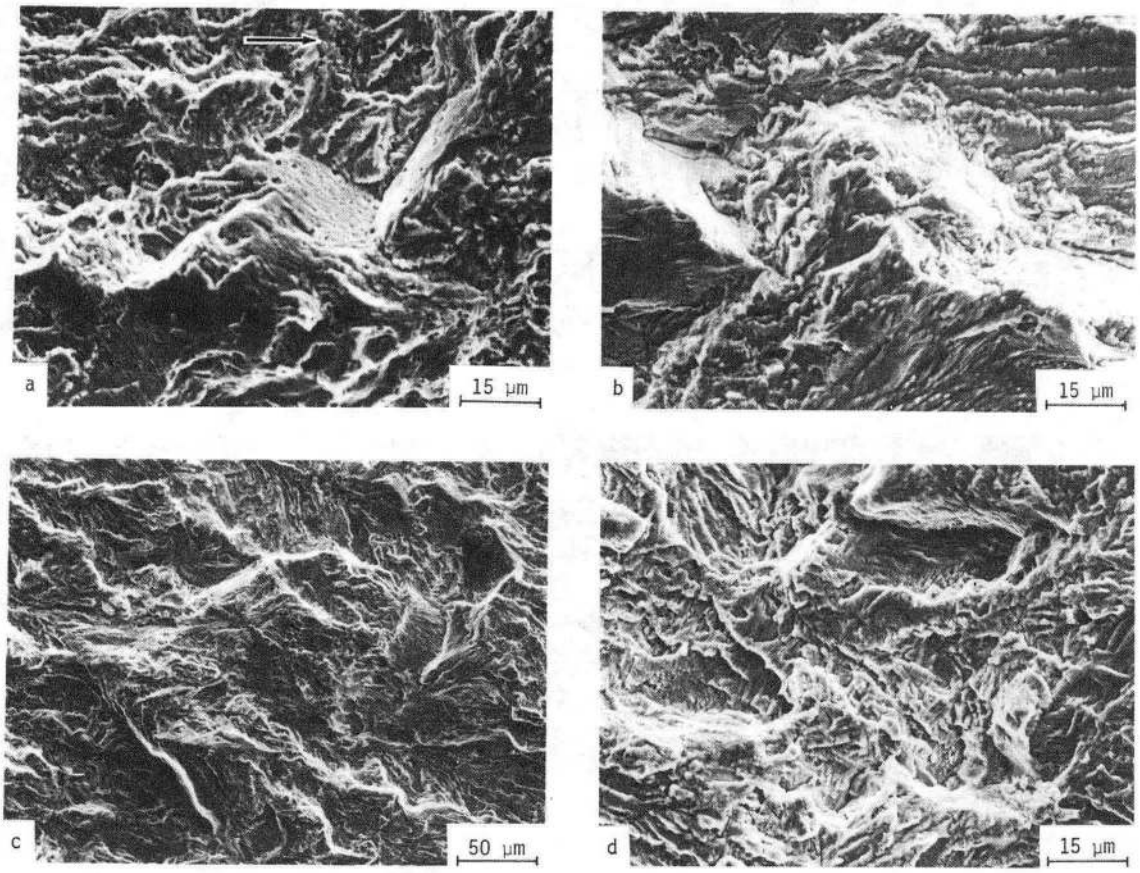

XBB 8610-7953

Fig. 5. Scanning electron micrographs of fatigue crack propagation in AISI 1008 steel in the duplex 26 pct martensite structure at a) ΔK = 21 MPa$\sqrt{m}$ (close to ΔK_{TH}), and b) ΔK = 30 MPa$\sqrt{m}$, and in the duplex 46 pct martensite structure at c) ΔK = 13 MPa$\sqrt{m}$ (close to ΔK_{TH}), and d) ΔK = 25 MPa$\sqrt{m}$. Arrow indicates general direction of crack growth.

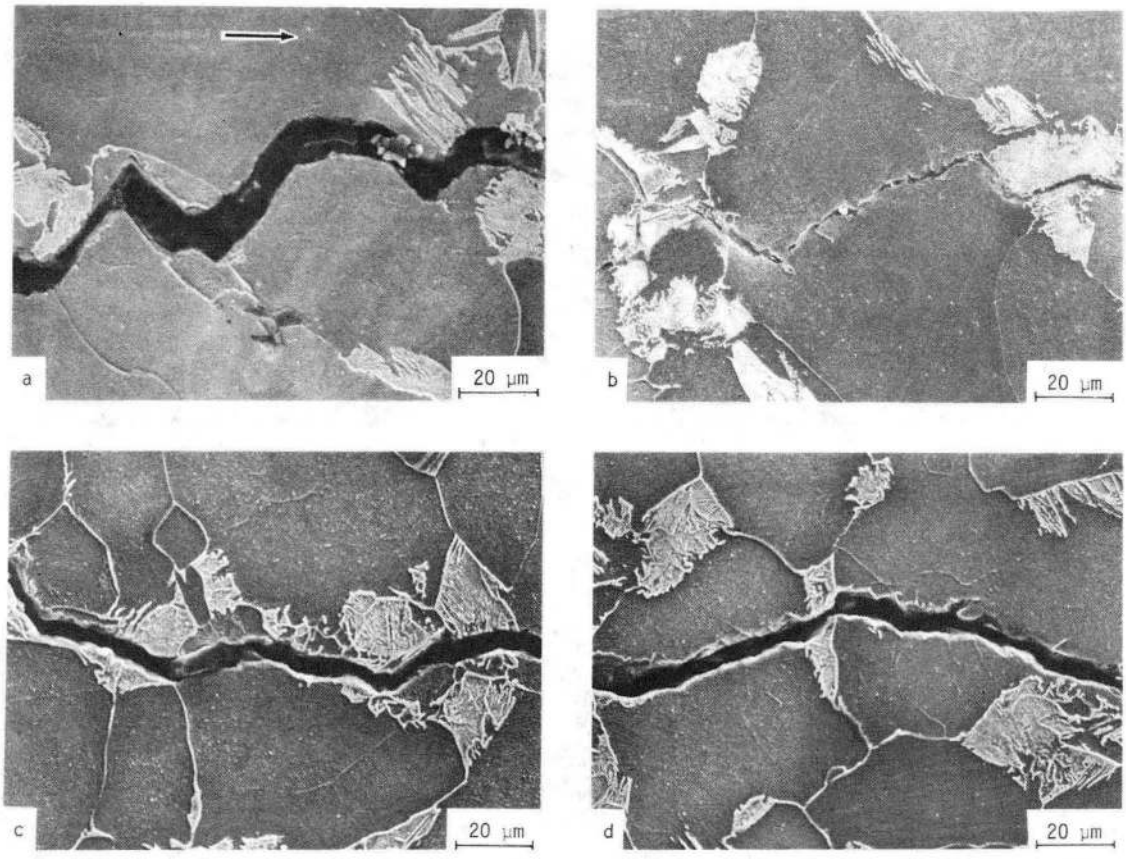

XBB 8610-7954

Fig. 6. Crack path profiles of fatigue crack propagation in AISI 1008 steel in the duplex 26 pct martensite structure at a) $\Delta K = 21$ MPa$\sqrt{m}$ (close to ΔK_{TH}), and b) $\Delta K = 30$ MPa$\sqrt{m}$, and in the duplex 46 pct martensite structure at c) $\Delta K = 13$ MPa$\sqrt{m}$ (close to ΔK_{TH}), and d) $\Delta K = 25$ MPa$\sqrt{m}$. Arrow indicates general direction of crack growth. (Etched in 2 pct nital). (The width of the crack may not be representative in these micrographs as crack path sections naturally must be taken following completion of the entire fatigue test.)

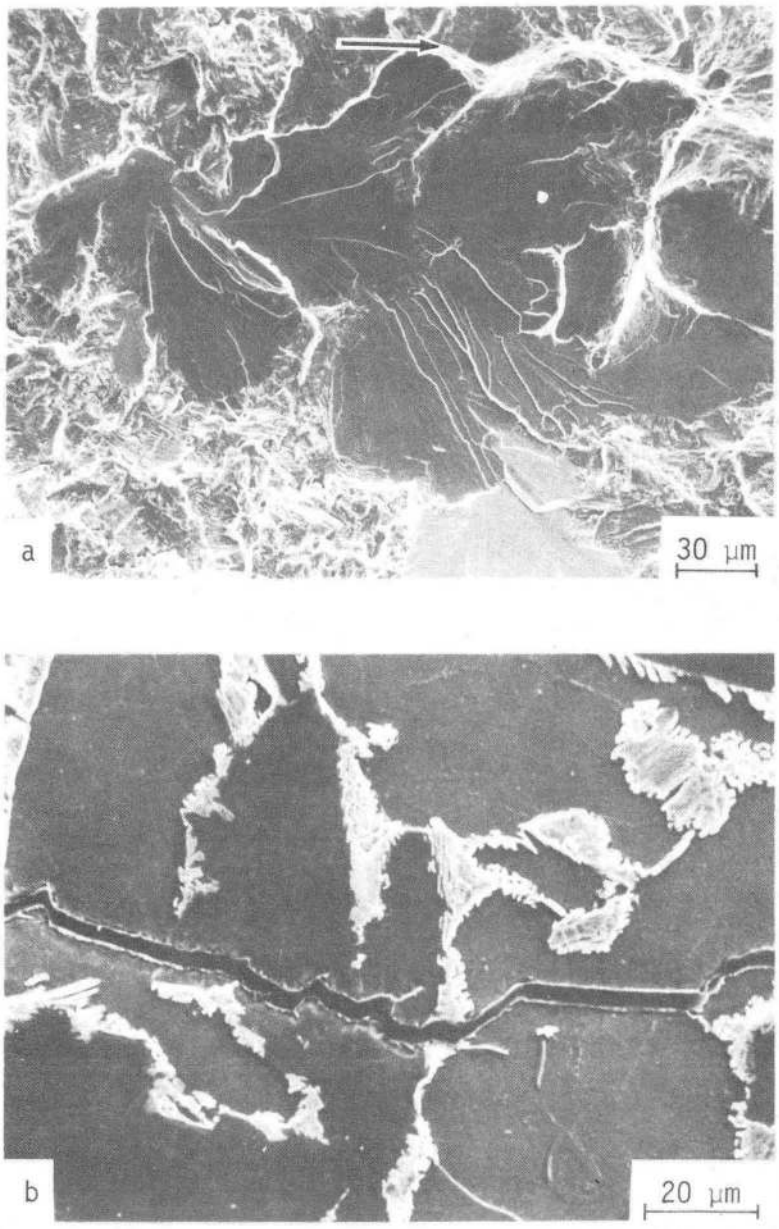

XBB 8610-7956

Fig. 7. a) Scanning electron fractograph and b) crack path profile showing cleavage fracture in the ferrite during fatigue crack propagation at ΔK = 25 MPa$\sqrt{m}$ in duplex 31 pct martensite microstructure in AISI 1015 steel. Arrow indicates general direction of crack growth. (Micrograph etched in 2 pct nital).

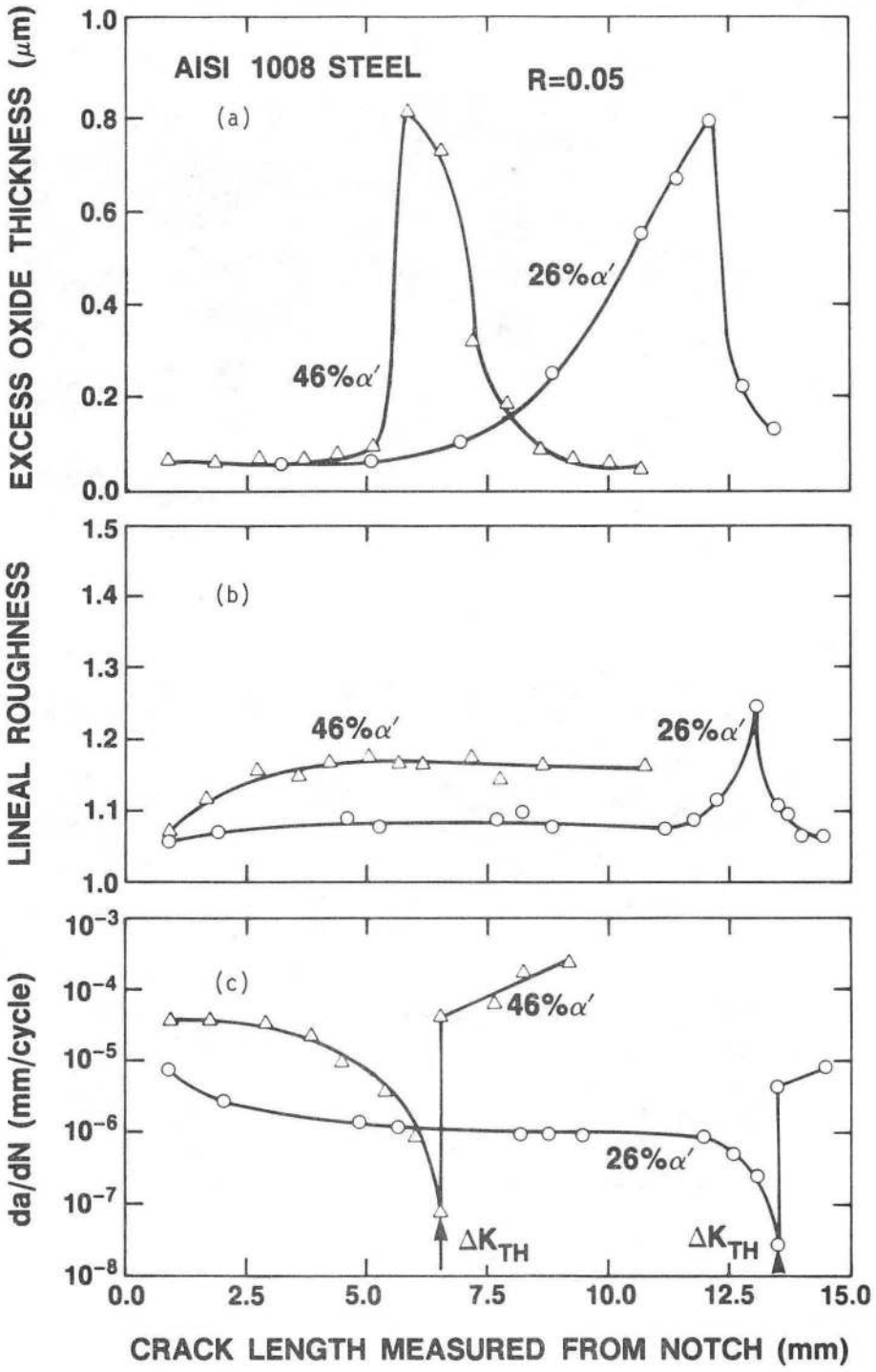

XBL 869-11699

Fig. 8. Variation in a) crack surface excess oxide thickness, b) fracture surface lineal roughness, and c) crack growth rate with crack length (measured from notch) for duplex 26 and 46 pct martensite microstructures in AISI 1008 steel.

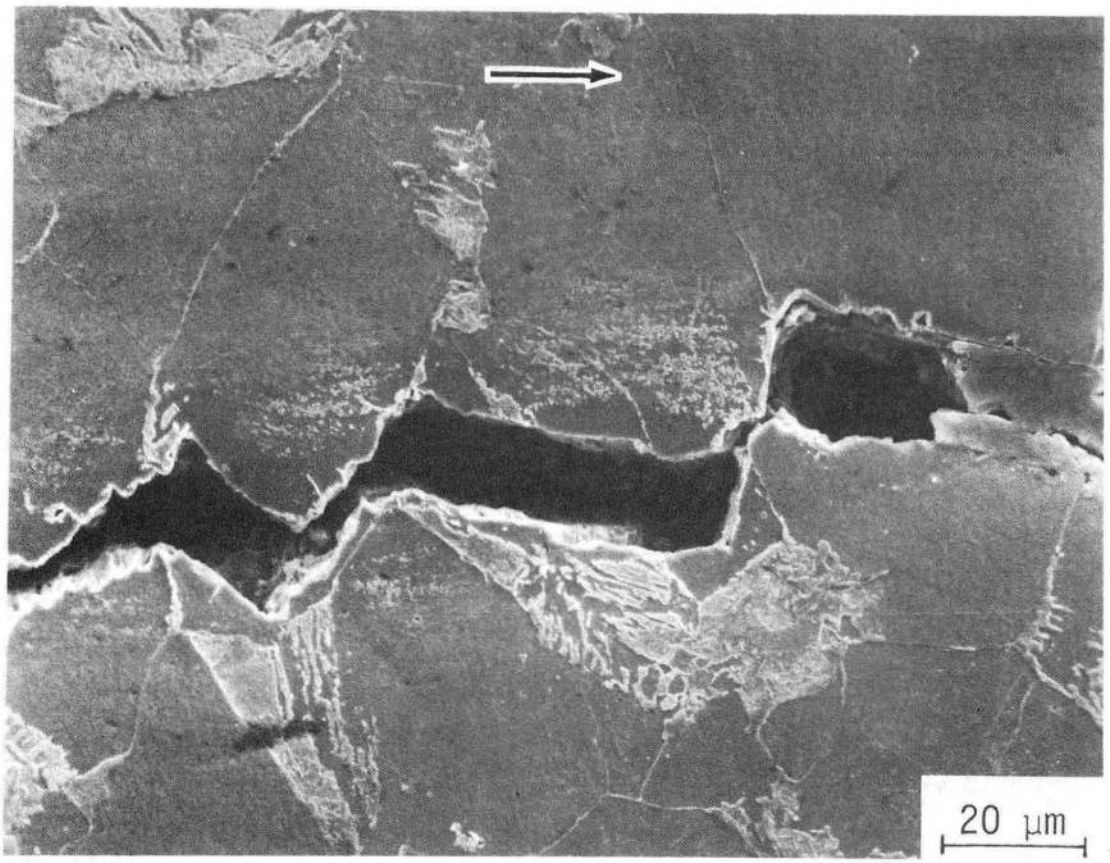

XBB 8610-7957

Fig. 9. Micrograph of the crack path morphology in dual-phase AISI 1008 steel, showing crack wedging from fracture surface asperity contact (roughness-induced crack closure), which is promoted by the deflected nature of the crack path. Arrow indicates general direction of crack growth. (Etched in 2 pct nital).

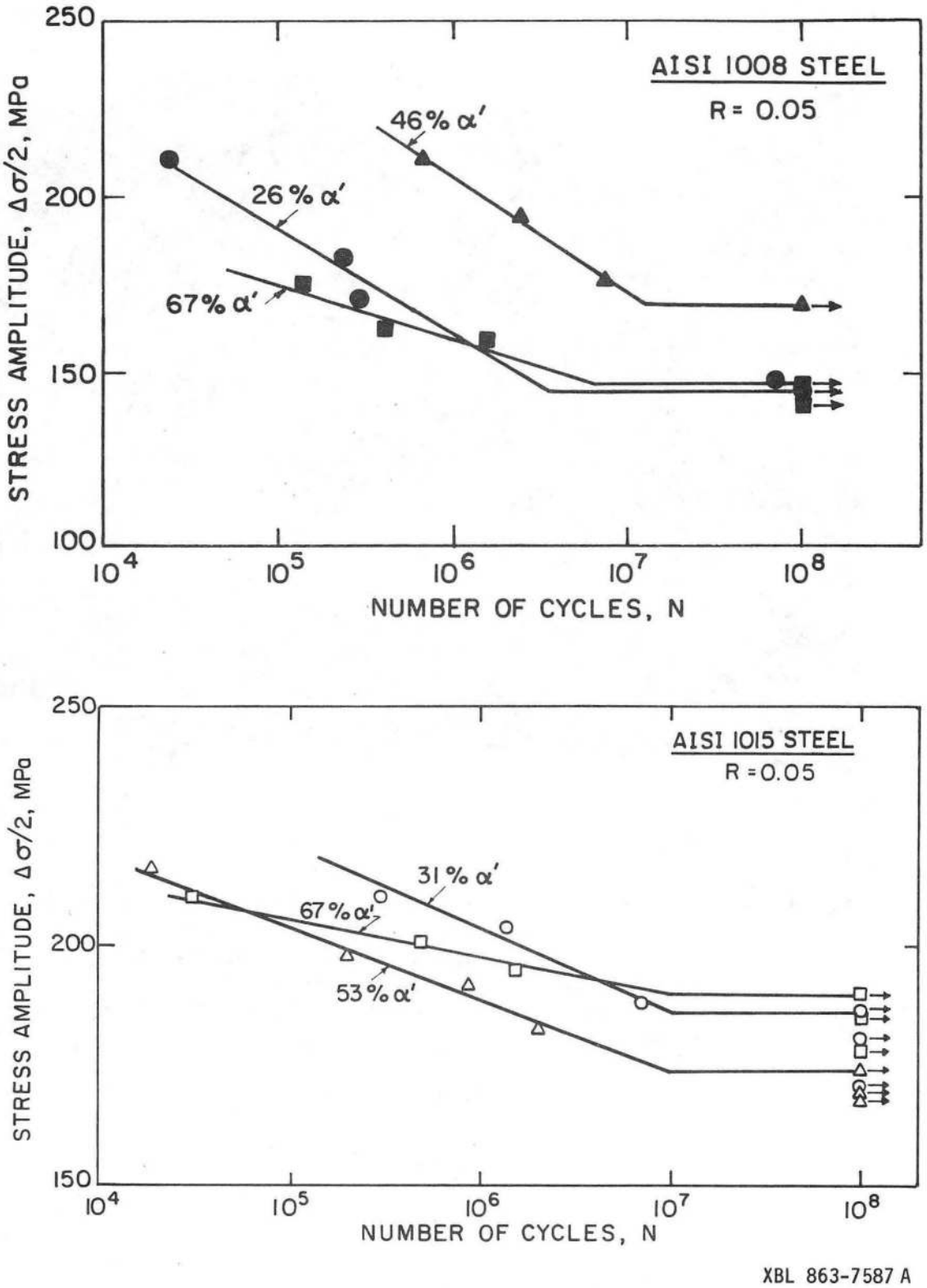

Fig. 10. Smooth bar S/N curves at R = 0.05 for duplex ferritic/martensitic microstructures in AISI 1008 and 1015 mild steels.

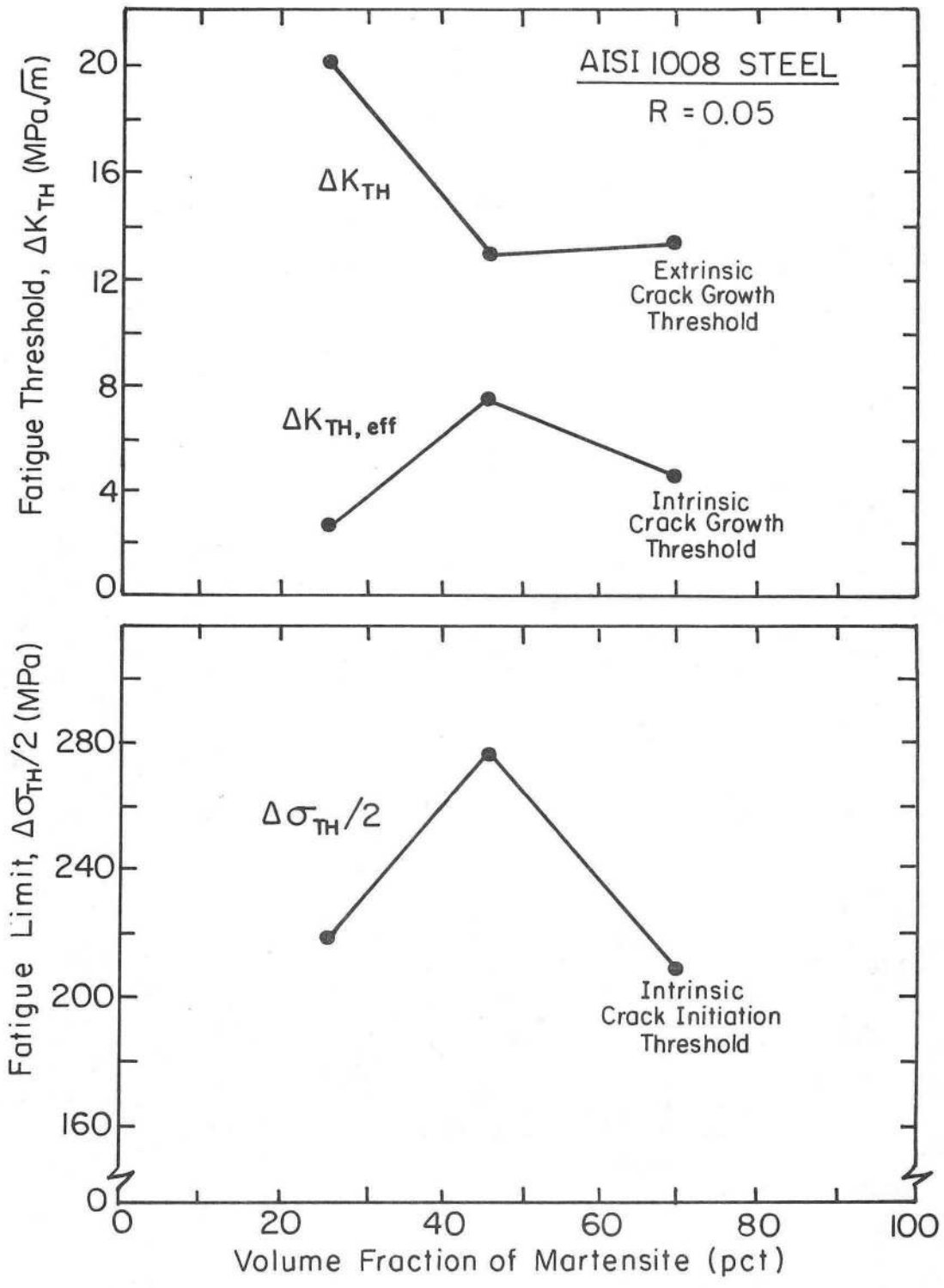

XBL 8510-6697

Fig. 11. Variation of nominal and effective fatigue crack growth thresholds (ΔK_{TH} and $\Delta K_{TH,eff}$, respectively) and smooth bar fatigue limits ($\Delta\sigma_{TH}/2$) with volume fraction of martensite for duplex ferritic/martensitic microstructures in AISI 1008 steel. Note that, whereas the nominal thresholds for crack initiation ($\Delta\sigma_{TH}/2$) and crack growth (ΔK_{TH}) show opposite dependencies on microstructure, when corrected for closure the crack initiation and growth thresholds ($\Delta\sigma_{TH}/2$ and $\Delta K_{TH,eff}$) show similar dependencies.

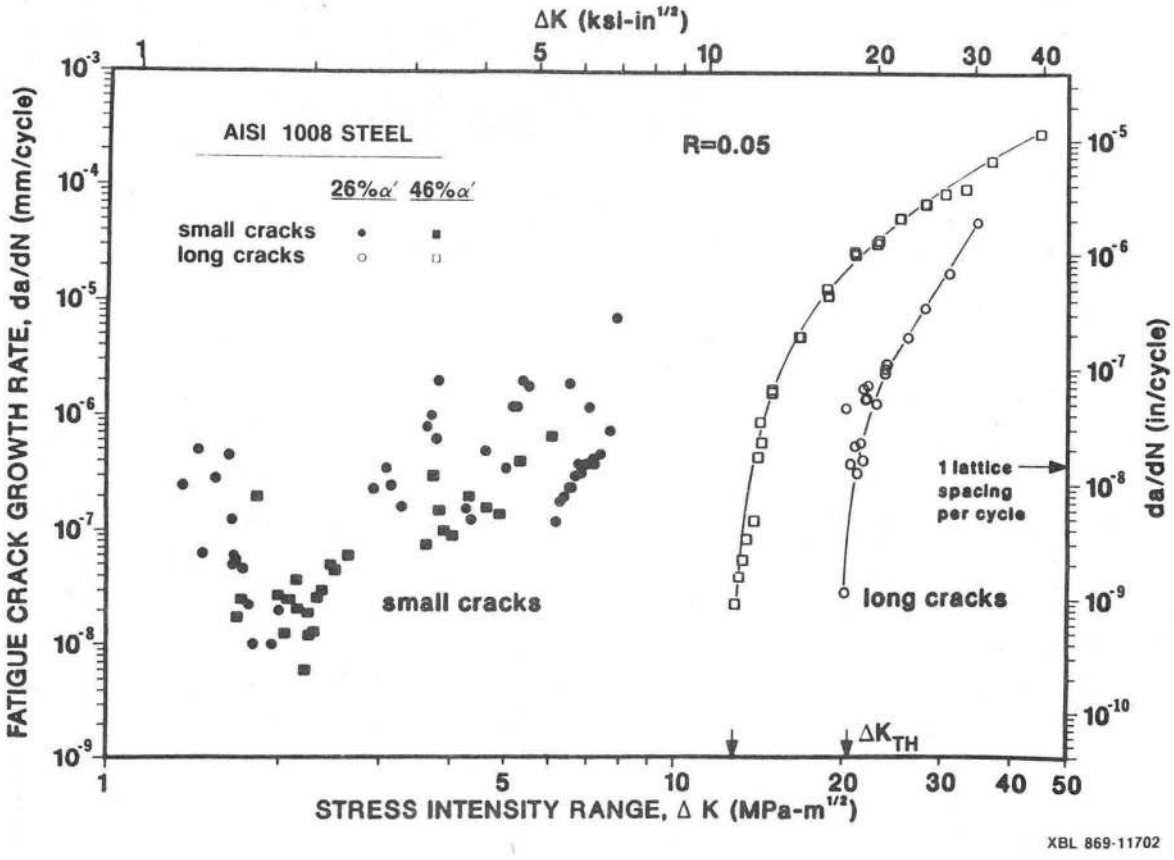

Fig. 12. Comparison of the fatigue crack growth rates of long ($\gtrsim$20 mm) and naturally-occurring small (10 to 1000 μm) cracks in duplex 26 and 46 pct martensite microstructures in AISI 1008 steel. Note how long crack growth rates (at fixed ΔK) are significantly slower in the 26 pct martensite structure, whereas small crack growth rates are marginally slower in the 46 pct martensite structure.

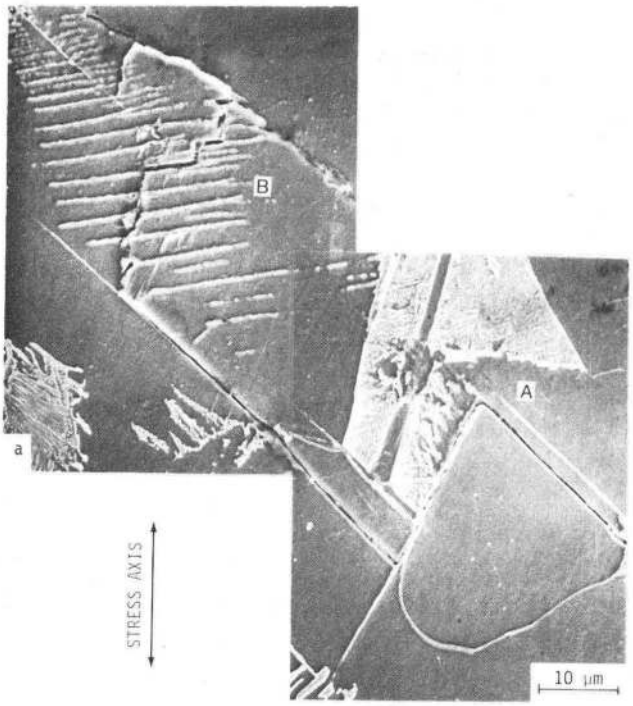

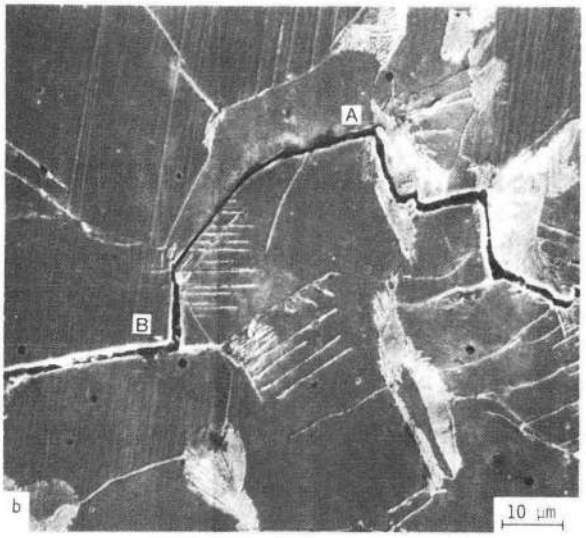

XBB 8610-7958

Fig. 13. Small fatigue crack growth in a) duplex 26 pct martensite and b) 46 pct martensite microstructures in AISI 1008 steel, showing preferential growth in the ferrite, abrupt crack deflection at the martensite phase (regions A), and slip band activity, blunting and deflection at ferrite grain boundaries (regions B). Arrow indicates direction of applied tensile stress. (Etched in 2 pct nital).

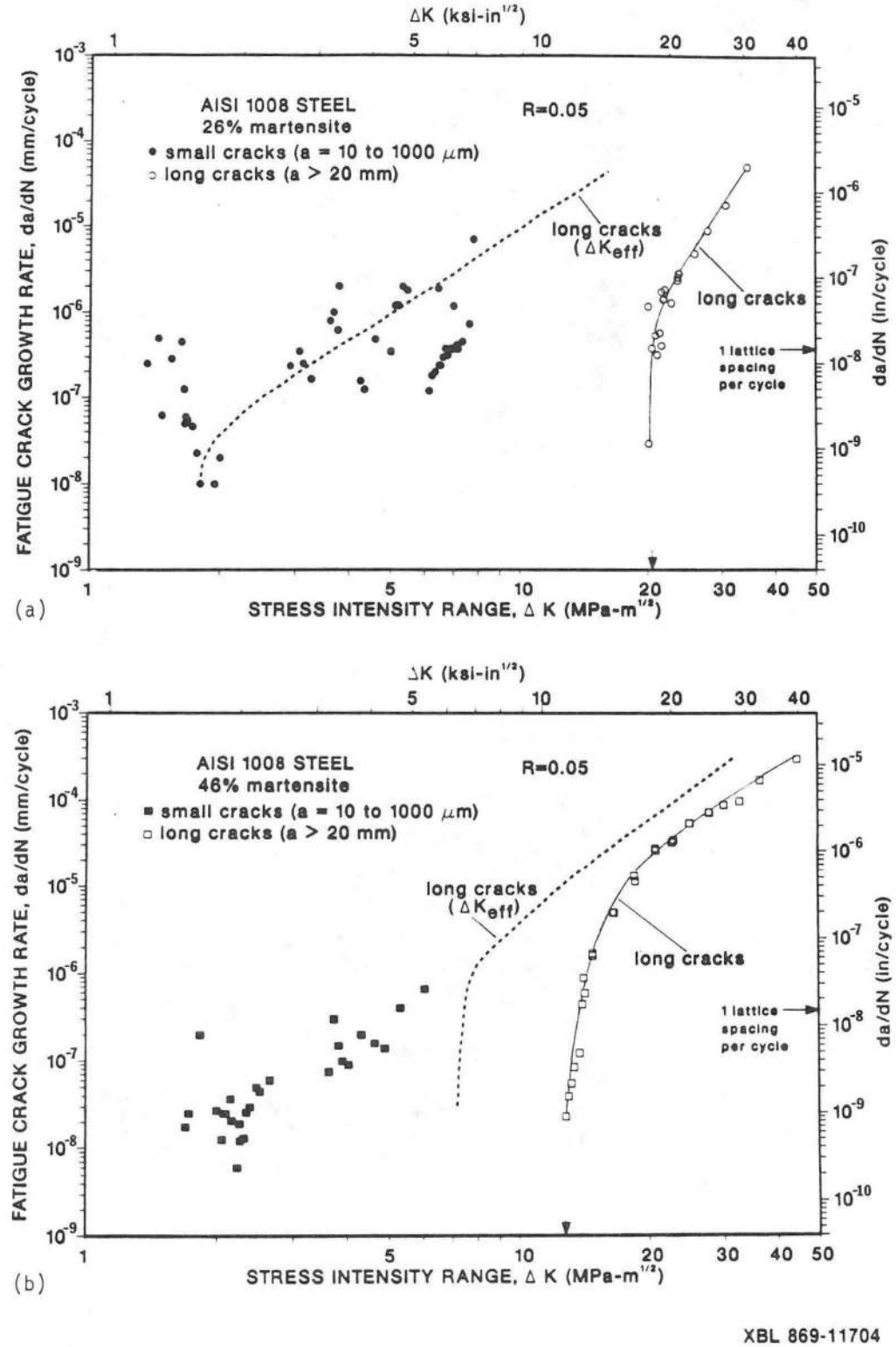

Fig. 14. Comparison of long (≳20 mm) and naturally-occurring small (10 to 1000 μm) fatigue crack growth in a) duplex 26 pct martensite and b) duplex 46 pct martensite microstructures in AISI 1008 steel as a function of nominal and effective stress intensity ranges (ΔK and ΔK_{eff}, respectively). Note the correspondence of long and small crack data when analysed in terms of ΔK_{eff} ($\Delta K_{eff} > \Delta K_{TH,eff}$).

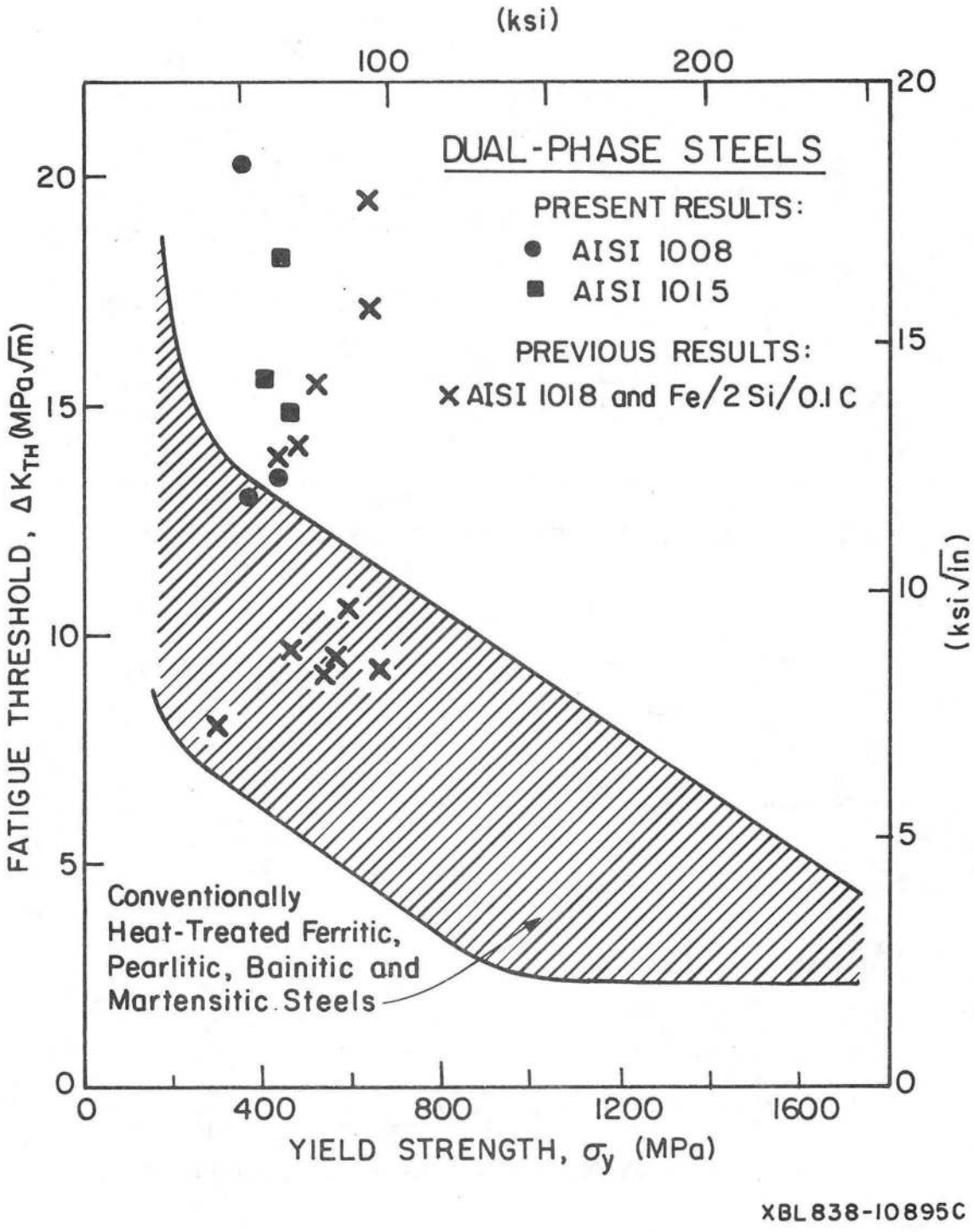

Fig. 15. Variation of long crack fatigue ΔK_{TH} thresholds (at low load ratios) with yield strength in steels, showing the superior fatigue/strength properties of dual-phase steels, compared to conventionally heat-treated ferritic, pearlitic, bainitic and martensitic steels. Threshold data obtained from refs. 18-23.

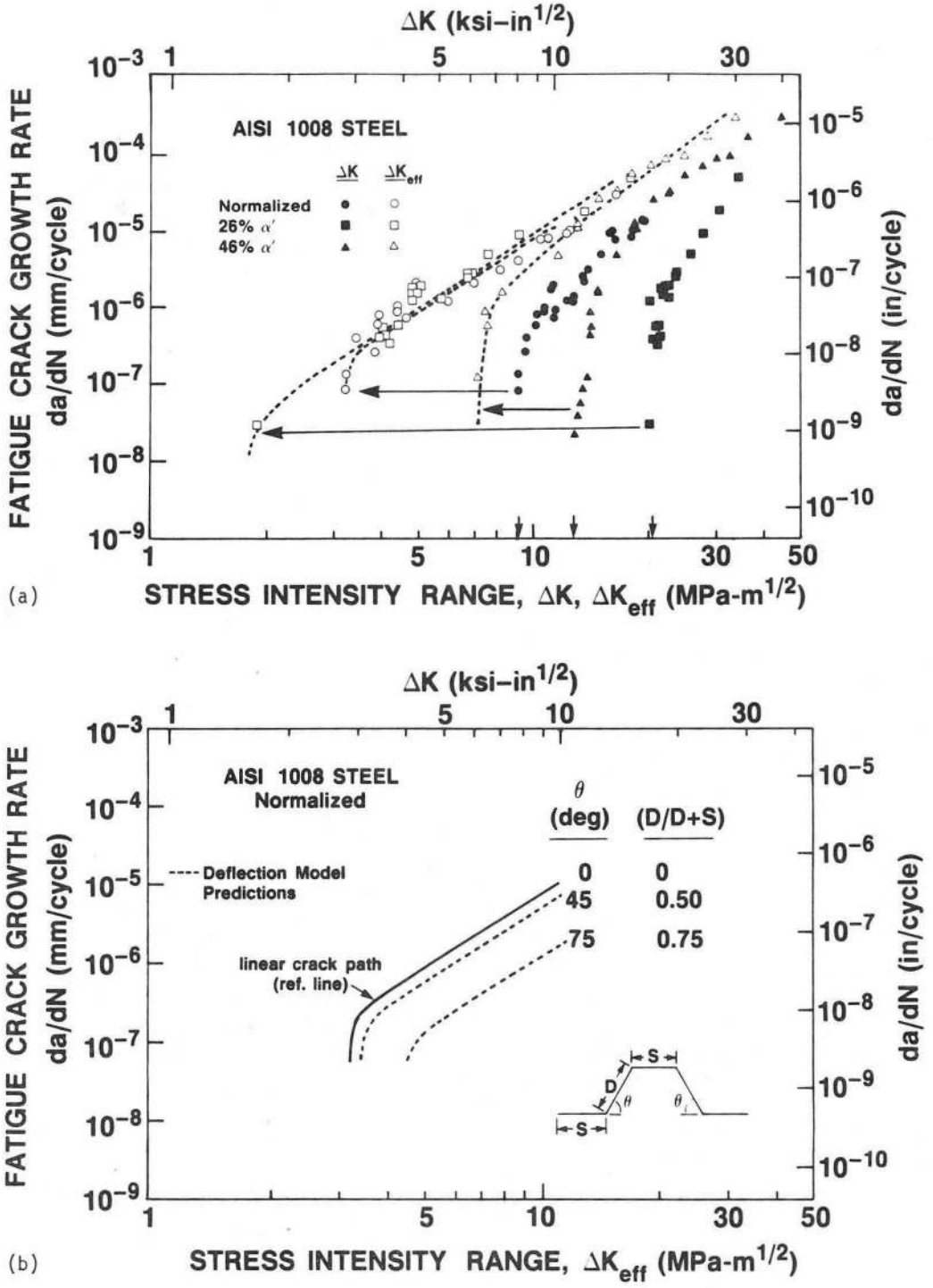

Fig. 16. Respective roles of crack closure and crack deflection in influencing long fatigue crack growth in duplex 26 and 46 pct martensite microstructures, compared to the normalized structure, in AISI 1008 steel, showing a) experimental da/dN data versus nominal ΔK (from Fig. 3a), corrected for closure in terms of da/dN versus ΔK_{eff}; and b) predictions of the effect of crack deflection, using two-dimensional linear elastic deflection model (Eq. 1 (7)), for θ between 0 and 75 deg with D/(D + S) between 0 and 0.75.

LAWRENCE BERKELEY LABORATORY
TECHNICAL INFORMATION DEPARTMENT
UNIVERSITY OF CALIFORNIA
BERKELEY, CALIFORNIA 94720